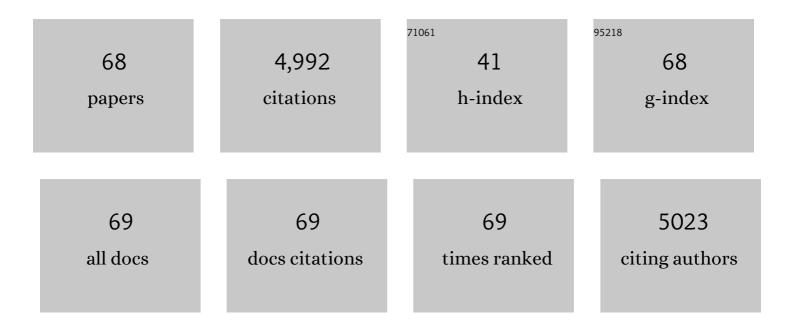
## List of Publications by Year in descending order

Source: https://exaly.com/author-pdf/4903100/publications.pdf Version: 2024-02-01



Hulm

#	Article	IF	CITATIONS
1	Electrically conductive polymer composites for smart flexible strain sensors: a critical review. Journal of Materials Chemistry C, 2018, 6, 12121-12141.	2.7	522
2	Ultrasensitive and Highly Compressible Piezoresistive Sensor Based on Polyurethane Sponge Coated with a Cracked Cellulose Nanofibril/Silver Nanowire Layer. ACS Applied Materials & Interfaces, 2019, 11, 10922-10932.	4.0	331
3	Highly Compressible and Robust Polyimide/Carbon Nanotube Composite Aerogel for High-Performance Wearable Pressure Sensor. ACS Applied Materials & Interfaces, 2019, 11, 42594-42606.	4.0	255
4	Superhydrophobic Electrically Conductive Paper for Ultrasensitive Strain Sensor with Excellent Anticorrosion and Self-Cleaning Property. ACS Applied Materials & Interfaces, 2019, 11, 21904-21914.	4.0	228
5	Flexible Sandwich Structural Strain Sensor Based on Silver Nanowires Decorated with Selfâ€Healing Substrate. Macromolecular Materials and Engineering, 2019, 304, 1900074.	1.7	187
6	Flexible conductive MXene/cellulose nanocrystal coated nonwoven fabrics for tunable wearable strain/pressure sensors. Journal of Materials Chemistry A, 2020, 8, 21131-21141.	5.2	176
7	Super light 3D hierarchical nanocellulose aerogel foam with superior oil adsorption. Journal of Colloid and Interface Science, 2019, 536, 245-251.	5.0	175
8	Cu <sub>3</sub> N Nanocubes for Selective Electrochemical Reduction of CO <sub>2</sub> to Ethylene. Nano Letters, 2019, 19, 8658-8663.	4.5	173
9	Wearable Strain Sensors Based on a Porous Polydimethylsiloxane Hybrid with Carbon Nanotubes and Graphene. ACS Applied Materials & Interfaces, 2021, 13, 15572-15583.	4.0	118
10	Photocatalytic dehydrogenation of formic acid promoted by a superior PdAg@g-C <sub>3</sub> N <sub>4</sub> Mott–Schottky heterojunction. Journal of Materials Chemistry A, 2019, 7, 2022-2026.	5.2	116
11	Porous Polyethylene Bundles with Enhanced Hydrophobicity and Pumping Oil-Recovery Ability via Skin-Peeling. ACS Sustainable Chemistry and Engineering, 2018, 6, 12580-12585.	3.2	109
12	Laccase immobilized polyaniline/magnetic graphene composite electrode for detecting hydroquinone. International Journal of Biological Macromolecules, 2020, 149, 1130-1138.	3.6	106
13	Solvent-free graphene liquids: Promising candidates for lubricants without the base oil. Journal of Colloid and Interface Science, 2019, 542, 159-167.	5.0	98
14	Electrostatic self-assembled NiFe2O4/Ti3C2Tx MXene nanocomposites for efficient electromagnetic wave absorption at ultralow loading level. Advanced Composites and Hybrid Materials, 2021, 4, 602-613.	9.9	97
15	Tunable magnetoresistance of core-shell structured polyaniline nanocomposites with 0-, 1-, and 2-dimensional nanocarbons. Advanced Composites and Hybrid Materials, 2021, 4, 51-64.	9.9	87
16	Hyperelastic magnetic reduced graphene oxide three-dimensional framework with superb oil and organic solvent adsorption capability. Advanced Composites and Hybrid Materials, 2020, 3, 473-484.	9.9	85
17	Flexible Conductive Polyimide Fiber/MXene Composite Film for Electromagnetic Interference Shielding and Joule Heating with Excellent Harsh Environment Tolerance. ACS Applied Materials & Interfaces, 2021, 13, 50368-50380.	4.0	85
18	Atomically Dispersed Cu Catalyst for Efficient Chemoselective Hydrogenation Reaction. Nano Letters, 2021, 21, 10284-10291.	4.5	85

#	Article	IF	CITATIONS
19	Tunable negative permittivity and magnetic performance of yttrium iron garnet/polypyrrole metacomposites at the RF frequency. Journal of Materials Chemistry C, 2019, 7, 3160-3167.	2.7	82
20	Enhanced electromagnetic wave absorption of engineered epoxy nanocomposites with the assistance of polyaniline fillers. Advanced Composites and Hybrid Materials, 2022, 5, 1769-1777.	9.9	78
21	Schiff-base-rich g-CxN4 supported PdAg nanowires as an efficient Mott–Schottky catalyst boosting photocatalytic dehydrogenation of formic acid. Rare Metals, 2021, 40, 808-816.	3.6	77
22	Shortâ€Range Diffusion Enables General Synthesis of Mediumâ€Entropy Alloy Aerogels. Advanced Materials, 2022, 34, .	11.1	74
23	Room-Temperature Chemoselective Reduction of 3-Nitrostyrene to 3-Vinylaniline by Ammonia Borane over Cu Nanoparticles. Journal of the American Chemical Society, 2018, 140, 16460-16463.	6.6	73
24	Alternating Multilayer Structural Epoxy Composite Coating for Corrosion Protection of Steel. Macromolecular Materials and Engineering, 2019, 304, 1900374.	1.7	71
25	Synergistically Toughening Polyoxymethylene by Methyl Methacrylate–Butadiene–Styrene Copolymer and Thermoplastic Polyurethane. Macromolecular Chemistry and Physics, 2019, 220, 1800567.	1.1	67
26	Biodegradable poly(lactic acid) nanocomposites reinforced and toughened by carbon nanotubes/clay hybrids. International Journal of Biological Macromolecules, 2020, 151, 628-634.	3.6	66
27	A resilient and lightweight bacterial cellulose-derived C/rGO aerogel-based electromagnetic wave absorber integrated with multiple functions. Journal of Materials Chemistry A, 2021, 9, 5566-5577.	5.2	62
28	Tunable sulfur vacancies and hetero-interfaces of FeS2-based composites for high-efficiency electromagnetic wave absorption. Journal of Colloid and Interface Science, 2021, 591, 148-160.	5.0	62
29	Eu <sup>2+</sup> â€Doped Layered Double Borate Phosphor with Ultrawide Nearâ€Infrared Spectral Distribution in Response to Ultraviolet–Blue Light Excitation. Advanced Optical Materials, 2022, 10, 2102204.	3.6	61
30	Engineering hierarchical heterostructure material based on metal-organic frameworks and cotton fiber for high-efficient microwave absorber. Nano Research, 2022, 15, 6841-6850.	5.8	59
31	Nitrogen-rich g-C3N4@AgPd Mott-Schottky heterojunction boosts photocatalytic hydrogen production from water and tandem reduction of NO3â^' and NO2â^'. Journal of Colloid and Interface Science, 2021, 581, 619-626.	5.0	58
32	Tunable negative dielectric properties of magnetic CoFe2O4/graphite-polypyrrole metacomposites. Advanced Composites and Hybrid Materials, 2022, 5, 899-906.	9.9	58
33	Solvent-free nanoalumina loaded nanocellulose aerogel for efficient oil and organic solvent adsorption. Journal of Colloid and Interface Science, 2021, 581, 299-306.	5.0	56
34	Room-temperature solid phase surface engineering of BiOI sheets stacking g-C3N4 boosts photocatalytic reduction of Cr(VI). Green Energy and Environment, 2022, 7, 66-74.	4.7	53
35	Thermally Conductive Anticorrosive Epoxy Nanocomposites with Tannic Acid-Modified Boron Nitride Nanosheets. Industrial & Engineering Chemistry Research, 2020, 59, 20371-20381.	1.8	51
36	Achieving enhanced electromagnetic shielding and absorption capacity of cellulose-derived carbon aerogels <i>via</i> tuning the carbonization temperature. Journal of Materials Chemistry C, 2020, 8, 5191-5201.	2.7	51

#	Article	IF	CITATIONS
37	Impedance response behavior and mechanism study of axon-like ionic conductive cellulose-based hydrogel strain sensor. Advanced Composites and Hybrid Materials, 2022, 5, 1812-1820.	9.9	50
38	Interfacial Engineering for High-Efficiency Nanorod Array-Structured Perovskite Solar Cells. ACS Applied Materials & Interfaces, 2019, 11, 33770-33780.	4.0	47
39	Hierarchical HCF@NC/Co Derived from Hollow Loofah Fiber Anchored with Metal–Organic Frameworks for Highly Efficient Microwave Absorption. ACS Applied Materials & Interfaces, 2022, 14, 2038-2050.	4.0	44
40	Enhanced electron transfer and light absorption on imino polymer capped PdAg nanowire networks for efficient room-temperature dehydrogenation of formic acid. Journal of Materials Chemistry A, 2018, 6, 1979-1984.	5.2	43
41	Chemical Synthesis of Magnetically Hard and Strong Rare Earth Metal Based Nanomagnets. Angewandte Chemie - International Edition, 2019, 58, 602-606.	7.2	42
42	Surface Pd-rich PdAg nanowires as highly efficient catalysts for dehydrogenation of formic acid and subsequent hydrogenation of adiponitrile. Journal of Materials Chemistry A, 2018, 6, 17323-17328.	5.2	41
43	High-density defects on PdAg nanowire networks as catalytic hot spots for efficient dehydrogenation of formic acid and reduction of nitrate. Nanoscale, 2017, 9, 9305-9309.	2.8	38
44	Amino-functionalized graphene oxide-supported networked Pd–Ag nanowires as highly efficient catalyst for reducing Cr(VI) in industrial effluent by formic acid. Chemosphere, 2020, 257, 127245.	4.2	38
45	Stabilizing Hard Magnetic SmCo <sub>5</sub> Nanoparticles by N-Doped Graphitic Carbon Layer. Journal of the American Chemical Society, 2020, 142, 8440-8446.	6.6	37
46	Bifunctional networked Ag/AgPd core/shell nanowires for the highly efficient dehydrogenation of formic acid and subsequent reduction of nitrate and nitrite in water. Journal of Materials Chemistry A, 2018, 6, 4611-4616.	5.2	35
47	Structure and magnetic properties of the porous Al-substituted barium hexaferrites. Journal of Magnetism and Magnetic Materials, 2021, 528, 167824.	1.0	34
48	The Properties and Preparation Methods of Different Boron Nitride Nanostructures and Applications of Related Nanocomposites. Chemical Record, 2020, 20, 1314-1337.	2.9	32
49	Conductive polyaniline hydrogel enhanced methane production from anaerobic wastewater treatment. Journal of Colloid and Interface Science, 2021, 581, 314-322.	5.0	31
50	FeCo alloy nanoparticle decorated cellulose based carbon aerogel as a low-cost and efficient electromagnetic microwave absorber. Journal of Materials Chemistry C, 2021, 10, 126-134.	2.7	30
51	One-pot formic acid dehydrogenation and synthesis of benzene-fused heterocycles over reusable AgPd/WO <sub>2.72</sub> nanocatalyst. Journal of Materials Chemistry A, 2018, 6, 23766-23772.	5.2	29
52	Enhanced dielectric properties of high glass transition temperature PDCPD/CNT composites by frontal ring-opening metathesis polymerization. Advanced Composites and Hybrid Materials, 2021, 4, 639-646.	9.9	25
53	Room-temperature hydrogen spillover achieving stoichiometric hydrogenation of NO3â^' and NO2â^' into N2 over CuPd nanowire network. Rare Metals, 2022, 41, 851-858.	3.6	23
54	Magnetically recyclable Sm2Co17/Cu catalyst to chemoselectively reduce the 3-nitrostyrene into 3-vinylaniline under room temperature. Nano Research, 2019, 12, 3085-3088.	5.8	20

#	Article	IF	CITATIONS
55	Bi-doped graphitic carbon nitride nanotubes boost the photocatalytic degradation of Rhodamine B. New Journal of Chemistry, 2022, 46, 3588-3594.	1.4	20
56	Facile preparation of a cellulose derived carbon/BN composite aerogel for superior electromagnetic wave absorption. Journal of Materials Chemistry C, 2022, 10, 5311-5320.	2.7	20
57	Size regulation and prediction of the SiO <sub>2</sub> nanoparticles prepared via Stöber process. Journal of Dispersion Science and Technology, 2017, 38, 70-74.	1.3	19
58	Activating the MoS <sub>2</sub> Basal Plane by Controllable Fabrication of Pores for an Enhanced Hydrogen Evolution Reaction. Chemistry - A European Journal, 2018, 24, 19075-19080.	1.7	17
59	Linking melem with conjugated Schiff-base bonds to boost photocatalytic efficiency of carbon nitride for overall water splitting. Nanoscale, 2021, 13, 9315-9321.	2.8	17
60	One-pot In Situ Microwave Hydrothermally Grown Zeolitic Imidazolate Framework-8 on ZnIn-Layered Double Oxides toward Enhanced Methylene Blue Photodegradation. Industrial & Engineering Chemistry Research, 2020, 59, 16637-16648.	1.8	11
61	Modulation of a solid-state reversible fluorescent photoswitching based on a controllable photochromic pyrazolones. Journal of Solid State Chemistry, 2014, 216, 73-78.	1.4	10
62	Chemical Synthesis of Magnetically Hard and Strong Rare Earth Metal Based Nanomagnets. Angewandte Chemie, 2019, 131, 612-616.	1.6	9
63	Regulating pH value synthesis of NiCo2O4 with excellent electromagnetic wave absorbing performance. Journal of Materials Science: Materials in Electronics, 2021, 32, 26059-26073.	1.1	9
64	Self-Assembled Bipolar Metals with Hollow Carbon Spheres for High-Performance Li–S Battery Cathodes. ACS Applied Energy Materials, 2021, 4, 12745-12753.	2.5	9
65	Tunable temperature-resistivity behaviors of carbon black/polyamide 6 /high-density polyethylene composites with conductive electrospun PA6 fibrous network. Journal of Composite Materials, 2019, 53, 1897-1906.	1.2	8
66	Single-organic component g-C3.6N4 achieves superior photoactivity antibacterial. Chemical Engineering Journal, 2022, 440, 135873.	6.6	8
67	A simple approach to porous low-temperature-sintering BaTiO3. Science China Chemistry, 2012, 55, 1765-1769.	4.2	2
68	Fluorescence modulation of a pyrazolone dye in the solid state based on energy transfer. New Journal of Chemistry, 2015, 39, 9866-9871.	1.4	2